DEVELOPING LSPR DESIGN GUIDELINES

D. Mortazavi[1, *], A. Z. Kouzani[1], A. Kaynak[1], and W. Duan[2]

[1]School of Engineering, Deakin University, Geelong, Victoria 3216, Australia

[2]School of Medicine, Deakin University, Geelong, Victoria 3216, Australia

Abstract—Applications of localized surface plasmon resonance (LSPR) such as surface enhanced Raman scattering (SERS) devices, biosensors, and nano-optics are growing. Investigating and understanding of the parameters that affect the LSPR spectrum is important for the design and fabrication of LSPR devices. This paper studies different parameters, including geometrical structures and light attributes, which affect the LSPR spectrum properties such as plasmon wavelength and enhancement factor. The paper also proposes a number of rules that should be considered in the design and fabrication of LSPR devices.

1. INTRODUCTION

Raman based biosensors work based on the scattered wave produced by analytes or biomolecules. Since the scattered wave is very weak for detection, the incident field must be first enhanced in a process called surface enhanced Raman scattering (SERS) [1]. The SERS method was initially discovered by Fleischmann et al. [2] in 1974. Later in 2005, Van Duyne et al. demonstrated that the Raman signal can be significantly enhanced when the Raman scatterer is placed near or on the surface of a roughened noble metal to realize the surface plasmon resonance (SPR) [3]. In SPR, the receptor molecule is immobilized on the surface of a metal film [4]. However, implementation of an array of SPR devices for real-time and parallel monitoring of multiple species is challenging. To overcome this difficulty, noble metal nano-particles are used instead of metal films to create localized surface plasmon

resonance (LSPR) [5]. The nano-plasmonic phenomenon happens when the particle permittivity is a complex function of frequency and its real part is negative in some frequencies, and the free-space wavelength is large in comparison with particle dimensions; these two conditions only occur in nano-scale [6]. In plasmonic or nano-plasmonic sensors, the extinction energy can be evaluated by the Lorentz-Mie theory for small spherical particles [7], but this theory is not satisfied for larger or non-spherical particles [8].

Tuning the plasmon or extinction spectrum is the main concern in designing nano-plasmoinc devices. The extinction spectrum can be controlled with a careful design of nano-particle geometries and incident wave attributes [9, 10]. This paper explores different parameters that influence the LSPR extinction spectrum. Understanding of these parameters would benefit the LPSR biosensor design procedures.

2. THEORETICAL BACKGROUND

Plasmon resonances can be often found experimentally by investigating metallic nanoparticles of complex shapes with radiation of various frequencies. Since this experimental investigations are very expensive, usually direct calculations of resonance characteristics is preferred. In this section, the calculation of the electromagnetic resonances of noble metal nanoparticles that are much smaller than the wavelength of the exciting radiation is discussed.

The electrostatic approximation is valid only when $\varepsilon_b(2\pi d/\lambda) <$ 1 [9], where ε_b is the electric permittivity of the background medium, λ is the incident light wavelength d and is the average diameter of the particle. According to this formula, for realizing the plasmon resonance in the visible wavelength range (380–750 nm) and in free air ($\varepsilon_b = 1$), we need to have particles with average size of less than 120 nm. In this case, because of the very small sizes, electrodynamics calculations are replaced with Laplace electrostatic formulas.

In addition to numerical methods, plasmon resonances have been experimentally investigated in metal self-assembled quantum dots [11, 12] and in nanoparticles of complex shapes [13, 14] by means of different techniques.

2.1. Electromagnetic Equations

To start with mathematical representations, assume a quasistatic approach using a spherical nano-particle of diameter d, which is much smaller than the incident light wavelength λ. Due to this small size

condition, the quasistatic estimation would be a good estimation for solving Maxwell's equations [15].

Assume that the metal nano-sphere with permittivity ε_m is embedded in a medium of permittivity ε_b. The incident electromagnetic wave $\mathbf{E}_0 = E_0\hat{\mathbf{z}}$ is taken along the z-axis, and independent of coordinates for distances at least as large as the sphere. Accordingly, the resulting field outside the sphere, $\mathbf{E_{out}}$, can then be written as [15–18],

$$\mathbf{E_{out}}\,(x,y,z) = E_0\hat{\mathbf{z}} - \alpha E_0 \left[\frac{\hat{\mathbf{z}}}{r^3} - \frac{3z}{r^3}\left(x\hat{\mathbf{x}} + y\hat{\mathbf{y}} + z\hat{\mathbf{z}}\right) \right] \tag{1}$$

where the first term is the applied field, and the second one is the induced dipole that results from polarization of the sphere electron density; also, x, y, and z are the usual Cartesian coordinates; r is the radial distance; $\hat{\mathbf{x}}$, $\hat{\mathbf{y}}$, and $\hat{\mathbf{z}}$ are the Cartesian unit vectors; and α is the metal dipole polarizability expressed as,

$$\alpha = ga^3 \tag{2}$$

where the LSPR dipole magnification factor g is defined as,

$$g = (\varepsilon_m - \varepsilon_b)/(\varepsilon_m + 2\varepsilon_b). \tag{3}$$

According to Eq. (3), the maximum enhancement occurs when the denominator of g approaches zero. Considering ε_{mr} and ε_{mi} as the real and imaginary parts of the metal nano-particle permittivity respectively, the plasmon resonance condition is fulfilled when $\varepsilon_{mr}(\omega) = -2\varepsilon_b$, thus from Eq. (1), the absolute square of $\mathbf{E_{out}}$ (at the surface of the sphere, i.e., at $r = a$) for a large g is given by,

$$E_{out}^2 = E_0^2 |g|^2 \left(1 + 3\cos^2\theta\right), \tag{4}$$

where θ is the angle between the applied electric field direction and the vector r that locates positions on the sphere surface. This indicates that the largest field intensities are obtained for angles θ equal to zero or $180°$, i.e., along the polarization direction; also, the ratio of the largest to smallest field enhancement versus θ is 4.

In Raman scattering, the incident electric field $\mathbf{E_0}(\omega)$ is magnified by the factor g during interaction with nano-particles to produce $\mathbf{E_1}(\omega)$. In striking the Raman scatterers, the magnified field $\mathbf{E_1}(\omega)$ then radiates an electric field with a shift in the incident wave frequency by the vibrational frequency ω' of the molecule (i.e., $\Delta\omega = \omega - \omega'$). The stoke-shifted field strikes the nano-particle again and emits the enhanced electric field $\mathbf{E_2}(\omega')$ with a magnification factor of g' similar to Eq. (3) [19, 20]. Accordingly, total Raman enhancement factor ε_R is defined as,

$$\varepsilon_R = \frac{|\mathbf{E_2}(\omega')|^2}{|\mathbf{E_1}(\omega')|^2} \frac{|\mathbf{E_1}(\omega)|^2}{|\mathbf{E_0}(\omega)|^2} \propto |g|^2 |g'|^2. \tag{5}$$

For small Stokes shifts, $|g|$ and $|g'|$ are maximized at approximately the same wavelength, so this is commonly referred to as E^4 enhancement or the fourth power of field enhancement at the nano-particle surface.

For larger particles, the higher multipoles term (especially the quadrupole term) becomes important to the extinction and scattering spectra as a result of phase retardation of the applied field inside the material [21]. In this case, using the same notation as above, the metal quadrupole polarizability is defined as,

$$\beta = g_q a^5, \tag{6}$$

where the LSPR quadrupole excitation enhancement factor is,

$$g_q = (\varepsilon_m \, \varepsilon_b)/(\varepsilon_m + 3/2 \, \varepsilon_b). \tag{7}$$

The mentioned collective modes are classified as "bright" or "dark" modes having finite or zero dipole moments, respectively. Bright plasmon modes, clearly visible in the optical spectrum, are excited by incident light, so they can radiate and their frequency spectrum is significantly broadened due to radiative damping. In contrast, dark modes do not couple efficiently to light, and therefore their spectrum cannot radioactively be broadened. The damping mechanism for dark modes is dominantly due to the imaginary part of the dielectric function of the metal. As a result, the light plasmon modes can be significantly wider than the dark plasmon modes [22].

The metal permittivity is size dependent and can be modelled in a function $\varepsilon_m(\omega, R) = \varepsilon_{IB}(\omega) + \varepsilon_D(\omega)$, as a combination of an interband term $\varepsilon_{IB}(\omega)$, accounting to the response of the d electrons, and a Drude term $\varepsilon_D(\omega)$ considering the free conduction electrons [23],

$$\varepsilon_D(\omega) = 1 - \frac{\omega_p^2}{\omega^2 + i\gamma\omega}, \tag{8}$$

where, ω_p is the bulk plasmon frequency. The phenomenological damping constant γ equals the plasmon bandwidth Γ for the case of a perfect free electron gas in the limit of $\gamma \ll \omega$. The damping constant γ, is a function of the particle radius r,

$$\gamma(r) = \gamma_0 + \frac{Av_F}{r} \tag{9}$$

where γ_0 is the bulk damping constant, v_F is the velocity of the electrons at the Fermi energy, and A is a theory-dependent parameter that includes details of the scattering process (e.g., isotropic or diffuse scattering) [23].

Although, the Drude term $\varepsilon_D(\omega)$ fits well with the metal permittivity for wavelengths above 600 nm, it is not a suitable model at resonance wavelengths below 600 nm, as shown in Figure 1. Due to
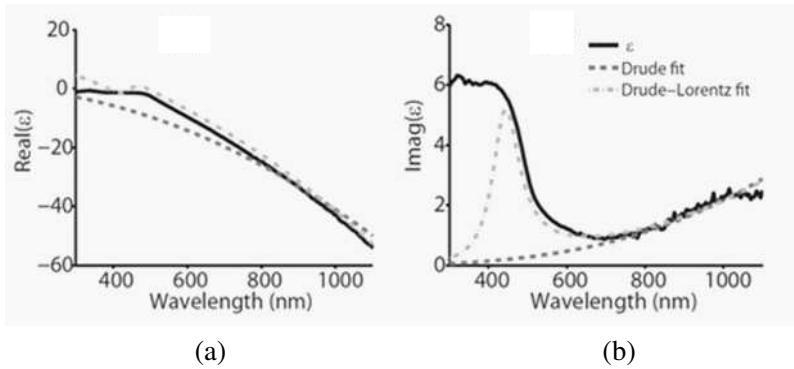
Figure 1. (a) Real and (b) imaginary parts of dielectric constant of gold versus Drude and Drude-Lorentz models [25].

the increase of the imaginary part of the electric permittivity at these high frequencies, interband transitions of the bound valance electrons $(\varepsilon_{IB}(\omega))$ come into play [24]. The result of this fit is shown as a dash-dotted curve in Figure 1.

Because of the above-mentioned deficiency of the Drude model and also instability of Fourier transform in the algorithm, the general Drude model modified by the Debye model [26], and the dispersion model (an extended version of the Debye model) [27] are utilized.

2.1.1. Nano-spheroids Modelling

The exact analytical electromagnetic solution of spheroidal particles is very complex; thus, usually numerical solutions of Maxwell's equations are discussed. For a spheroid with major axis of $2b$ and minor axis of $2a$, when an electric field $\mathbf{E}_0$, polarized along the major axis, strikes the particle, the Raman enhancement factor is given by Zeman and Schatz [28] as follows

$$g = \frac{\varepsilon_m - \varepsilon_b}{\varepsilon_m + \chi\varepsilon_b}, \tag{10}$$

And the shape factor parameter χ is given by,

$$\chi = -1 + \frac{1}{(\xi_0^2 - 1)\left[\frac{\xi_0}{2}\ln\left(\frac{\xi_0 + 1}{\xi_0 - 1}\right) - 1\right]}. \tag{11}$$

where

$$\xi_0 = \left(1 - \frac{a^2}{b^2}\right)^{-1/2}. \tag{12}$$

Eq. (10) is a generalization of Eq. (3) where the constant value 2 has been replaced by the shape factor χ. In fact, the parameter χ equals 2 for a sphere, but for prolate spheroids where $b > a$ ($\xi_0 > 1$), χ is larger than 2, and for oblate spheroids where $b < a$ ($\xi_0 < 1$), it is less than 2. In this polarization direction (along the major axis of the spheroid), a dipole resonance on the surface of the spheroid is generated due to the angular momentum l that is equal to one. According to Eq. (10) the condition for realizing this resonance is $\mathrm{Re}(\varepsilon_m + \chi\,\varepsilon_b) = 0$. Therefore, in prolate spheroids (when $\chi > 2$), the plasmon resonance red-shifts with respect to a sphere, because for metals, the real part of ε_m is more negative for longer wavelengths (see Figure 1(a)). However, in oblate spheroids (when $\chi < 2$), the polarization of the incident field is parallel to the symmetry axis of the spheroid, and thus other resonances are generated due to multipoles ($l \geq 2$). For a sphere $\chi = 2$; thus the dipole resonance generated when $\mathrm{Re}\,(\varepsilon_m) = -2\,\varepsilon_b$, and the quadrupoles ($l = 2$) are generated when $\mathrm{Re}\,(\varepsilon_m) = -1.5\varepsilon_b$. These factors arise from the exponents in the radial solutions to Laplace's equation, e.g., the factors r^l and $r^{-(l+1)}$. For dipole excitation ($l = 1$), the magnitude of the ratio of the exponents is $(l + 1)/l = 2$, while for quadrupole excitation, ($l = 2$), we have $(l + 1)/l = 1.5$ [29].

   In multipole modes, the expression for g in Eq. (10) still applies, but the expression for χ is as follows [15],

$$\chi = -1 - \frac{1}{\left[\dfrac{\xi_0}{2}(\xi_0^2 - 1) \ln\left(\dfrac{\xi_0 + 1}{\xi_0 - 1}\right) - \xi_0^2 \right]}. \tag{13}$$

In addition, like sphere case, increasing the dielectric constant of the external medium, ε_b, leads to additional red-shifting of the plasmon resonances [28], also as spherical case, this relation demonstrates that maximum enhancement is achieved along the polarization direction [15].

3. LSPR DESIGN PARAMETERS

Tuning LSPR parameters in probing different biomolecules is very important because maximum sensitivity and accuracy can be achieved. In this section, the most important parameters affecting the plasmon spectrum are described. This section provides the knowledge that is required to design and fabricate a LSPR device suitable for biosensing applications.

3.1. LSPR Design Parameters, Size Effect

The nano-particle size has two different impacts on the plasmon, (i) if the nano-particle is small enough (less than 20 nm for gold), the intrinsic effect of the particle directly affect the metal permittivity $\epsilon(\omega, R)$; (ii) if the particle is not small enough (larger than 25 nm for gold), the extrinsic effect is enabled, where the extinction coefficient is dependent on the size r.

Figure 2 demonstrates the intrinsic and extrinsic effects for gold nano-particles. This size dependence is considered in the Drude model expressed by Eq. (8).
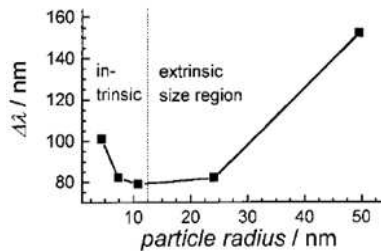

Figure 2. Size effect on the plasmon bandwidth of spherical gold nano-particles [23].

Figures 3(a) and (b) show extinction spectrum of a nano-sphere in vacuum for two different sizes of 30 and 60 nm, respectively, calculated using Mie theory. For smaller nano-spheres, only one peak is observed which is due to the dipole surface plasmon resonance. However, larger nano-spheres present two peaks in the plasmon resonance where the first one, which occurs in the UV range, is due to the quadrupole plasmon resonance.

In Section 2.1.2, it has been already explained how multipole resonance wavelengths drop for higher modes $l \geq 2$. It is obvious that the dipole plasmon wavelength changes with the size of nano-particles. The reason for this change can be found in the damping constant in the Drude model in Eq. (8) that is dependent on the particle size (see Eq. (9)). Due to redistributes of free electrons between the particle surface and bulk phase when increasing the size of the nanoparticles, the plasmon wavelength red-shifts and broadens at the resonant peak, leading to the increase of extinction efficiency [30].

Another parameter that affects the nano-spheres spectrum is their interaction with their substrate. In an investigation, a supporting nano-pillar with heights of 20 and 40 nm have been used to fabricate a typical Au nano-disk on a glass substrate. The experiments show
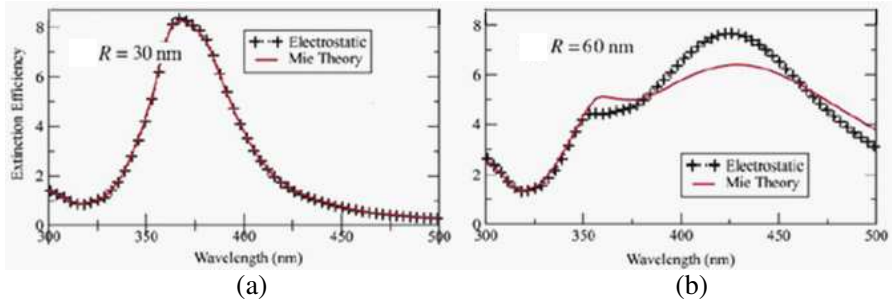
Figure 3. Extinction efficiency for a silver sphere of diameter (a) 30 nm and (b) 60 nm [29].

that the RI sensitivity (defined as $S = (\lambda_m - \lambda_{air})/(n_m - n_{air})$) or the LSPR peak shift per refractive index unit (RIU) against the resonance wavelength remarkably rises as the height of the supporting pillars increases [31, 32].

3.2. LSPR Design Parameters, Multi-particle Interaction Effect

The potential energy of an assembly of nano-particles is the sum of the potential energies of the primitive plasmons of each nano-particle, which may include coupling between primitive plasmon modes of different l and m, where l is the angular momentum of individual nano-particles, and m is the multipolar orientation, i.e., $m = 0$ means plasmons polarized along the main axis and $m = \pm 1$ means plasmons polarized perpendicular to the main axis [33]. One of the approaches to consider these interactions is the plasmon hybridization (PH) method, where all angular momentum orders in the plasmon calculations are considered.

It is generally necessary to tune the plasmon energies; however, the frequencies of the plasmon resonances of small nano-particles are scale invariant in the dipole limit. Therefore, multi-particles (e.g., dimers or nano-shells) are introduced; the gap distance between them are modified to tune the plasmon energies [34]. This gap produces "hot spots", where surface plasmons interact mutually, and thus, provide the hottest point of the plasmon signal. Therefore, if a target molecule trapped in these hot spots, we will get the highest Raman enhancement signal [27, 35].

3.2.1. Nano-structures

Here nano-structures including dimers (Figure 4(a)), nano-hemisphericals (Figure 4(b)), and nano-cuboids (Figure 4(c)) are evaluated to analyse multi-particle interactions effect.
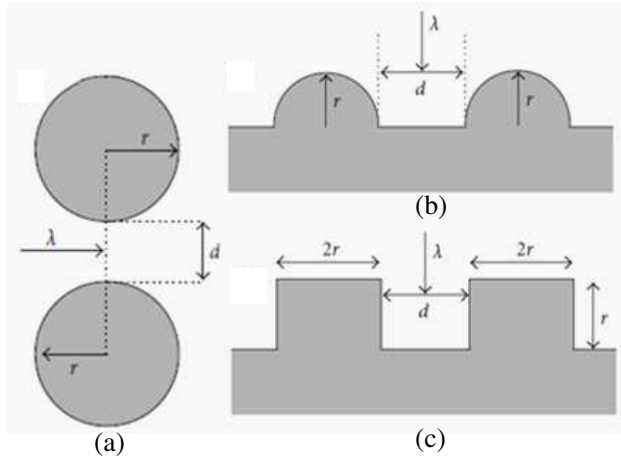

Figure 4. Section of a (a) dimer, (b) hemispherical structure, and (c) cuboid structure [36].

The main reason of increasing the Electromagnetic enhancement factor in dimers compared with the singlets is due to two factors, firstly the coupling of singlet resonances in the dimer case, and secondly localizing the potential drop to a confined region for the two nano-particles [37]. It is shown in Ref. [38] that large interparticle coupling effects can be achieved in LSPR substrates fabricated with electron-beam lithography.

Figure 5 shows both FDTD and MEM analysis on the magnitude of the enhanced electric field in a gold dimer versus spacing. It can be easily seen that the maximum enhancement occurring between wavelengths 546–560 nm, increases with decreasing the spacing [27, 36].

Figure 6 also explains FDTD and MEM results on the effect of increasing diameter of the gold nano-particles forming the dimers on rising the enhancement factor as expressed in the above rule.

It has been shown that the interaction between hemispheres become more important when hemispheres are brought closer than about 3 times the radius of individual semicylinders ($d < 3R$), but below a separation of $d = 3R$ the interaction grows rapidly [39]. The results from the modelling of the nano-structured show that the enhancements of hemisphericals are higher than those for the other
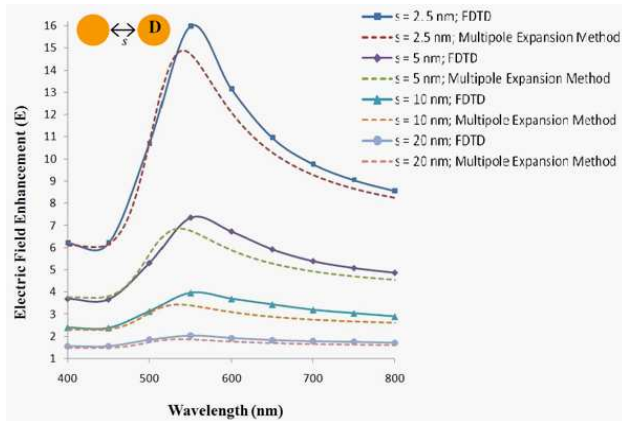
Figure 5. The effect of the spacing s on the magnitude of the enhanced electric field [27].
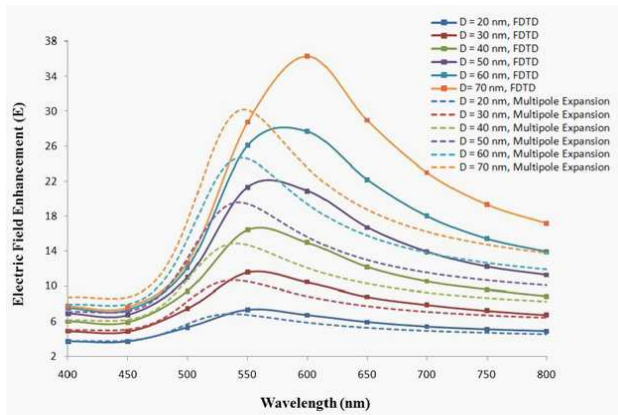
Figure 6. Effect of nano-spheres diameter forming a dimer on electric field enhancement, evaluated by employing FDTD simulations and MEM for the spacing $s = 5$ nm [27].

nano-structures at shorter wavelengths, but drop off more quickly as the wavelength increases and are generally lower than those observed for the two nanoparticles at longer wavelengths [40]. Also, experiments on the structured surfaces show that when the hemispheres are overlapping $(d < r)$, the maximum Raman enhancement is similar to when the hemispheres are well separated $(d > 3r)$. However, when the hemispheres are close to each other, at $d = 2r$ or $2r + 1$ nm, much

larger Raman enhancements are predicted [36].

Isolated nano-particles introduce enhancement factors of $\varepsilon_R = 10^4$, Larger values of $\varepsilon_R = 10^8$ can be achieved using dimers of silver nano-particles [27, 39, 41]. To achieve more enhancements, an array of nano-spheres or dimers can be employed. A one-dimensional array of 50 nm spheres (the polarization and wave-vector of the incident light is assumed to be perpendicular to the array) with spacing of 450 nm to 500 nm introduces very sharp peaks in the extinction spectrum due to dipolar interactions between the particles. This structure introduces an enhancement of $\varepsilon_R = 10^6$, indicating an extra factor of 10^2 is produced as a result of the long-range electrodynamic interactions [41]. If an array of dimers with optimized spacing is employed, a higher enhancement of $\varepsilon_R = 10^9$ can be attained. In addition, using an array of dimers of truncated tetrahedrons leads enhancement estimates of $\varepsilon_R = 10^{13}$. Further, a two-dimensional array of dimers show larger electromagnetic enhancement factors on the order of $\varepsilon_R = 10^{13-14}$ [41].

Like dimers, FDTD simulation of a combination of three different sized silver nano-spheres with polarization parallel to the axis of the symmetry shows the maximum field enhancement of about 300 in hot spots [26].

3.2.2. Trimers and Quadrumors

An experiment done to investigate the plasmon energy peaks of a quadrumor (four identical nano-spheres on the vertices of a square) and a trimer (three identical nano-spheres on the vertices of an equilateral triangle) shows that the two lowest-energy peaks of the plasmon refer to $l = 1$ and higher-energy resonances are for $l = 2$ and $l = 3$. Also, it is shown that there is a large effect in the plasmonic structure of the trimer when the symmetry is broken; however, the quadrumor appears quite robust for the perturbations [42].

In a work done by Hongxing Xu et al., it is shown that any aggregates of nano-particles such as silver trimers in the simplest case, significantly modulate the polarization of the scattered light, when a single-molecule Raman scatterer located in the gap between two of the nanoparticles. In this case, the third nano-particle acts as a wavelength-dependent polarization rotator; the rotation degree depends on the size of this particle and its distance from the other ones. Thus, trimers can be used for precise control of light polarization on the nanoscale [43].
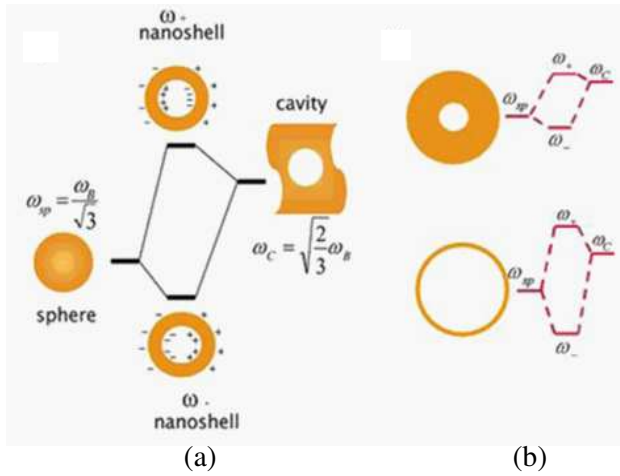
Figure 7. (a) plasmon hybridization in metal nano-shells, and (b) the effect of shell thickness on plasmon frequencies [45].

Figure 8. Schematic of a nano-rice [45].

3.2.3. Nano-shells

Nano-shell plasmon resonances result from the interaction between the plasmon response of a sphere and that of cavity (Figure 7(a)). The strength of these resonances is controlled by the thickness of the metal shell layer (Figure 7(b)). This interaction results in the splitting of the plasmon resonances into two new resonances, the lower energy symmetric plasmon (ω_{l-}) and the higher energy antisymmetric plasmon (ω_{l+}), for each $l > 0$. The lower energy plasmons interacts strongly with the incident field compared to weak interaction of the higher energy plasmons. Therefore, the energy of the optically active plasmon resonance is shifted to lower energies (lower frequencies) with decreasing shell thickness [44].

3.2.4. Nano-rices

Plasmon tunability in nano-rices (Figure 8) arises from varying the thickness of the shell layer. It is shown that decreasing the shell

layer thickness red-shifts the plasmon resonance and decreases the quadrupole resonance extinction [45, 46].

Extinction efficiency of ellipsoidal (39, 48) nm (minor axis = 39 nm, major axis = 48 nm) silver nano-shells shows that if the incident electric field is polarized along the minor axis of the nano-rice, the extinction cross section is blue-shifted with increasing distortion; however, if the incident electric field is polarized along the long axis, the extinction cross section is red-shifted with increasing distortion [47].

3.2.5. Nano-eggs

In a nano-shell with the same center for both inner and outer shells, plasmon hybridization between cavity and sphere components only occur at the same angular momentum l ($\Delta l = 0$) (see Figure 9(a)). However, in the nano-eggs holding any offset between the centers of the shells, other angular momentums can contribute to the bonding and antibonding plasmon modes as shown Figure 9(b).

(a)   (b)
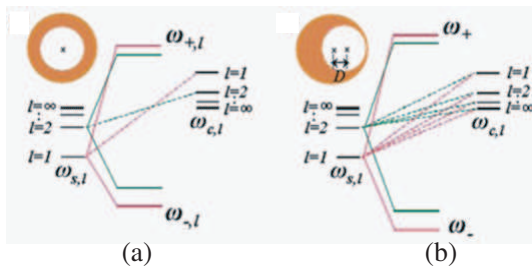
Figure 9. Schematic of plasmon hybridization in (a) a concentric nano-shell, and (b) a nano-egg [45].
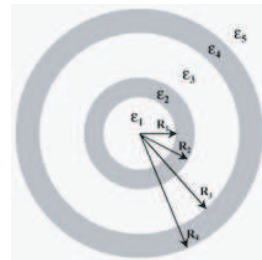
Figure 10. Schematic of a Nano-matryushkas [48].

$|\omega_-^-\rangle$ $|\omega_-^+\rangle$ $|\omega_\perp^-\rangle$ $|\omega_\perp^+\rangle$
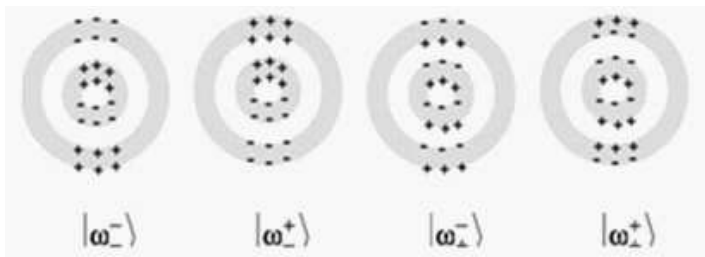
**Figure 11.** Induced polarization modes of the Nano-matryushkas [48].

3.2.6. Nano-matryushkas

Another structure, entitled nano-matryushkas (Figure 10), is fabricated using four-layer concentric nano-shell particles. This structure helps us to independently tune the energies of the inner shell and outer shell plasmons by controlling the strength of the interaction between the inner and outer shell plasmons, which is in turn makes its overall resonant response on the outer surface controllable for putting the target molecules on the outer surface. In this structure, ε_1 and ε_3 are composed of SiO_2; ε_2, ε_4 are composed of Au; and ε_5 is the embedding medium.

Figure 11 shows the interaction between symmetric antibounding energy (ω_{l+}) and anti-symmetric bounding energy (ω_{l-}) of the inner and outer metal shells for dipole excitation ($l = 1$). Four different hybridizations of the dipole moments at the metallic interfaces of the concentric nano-shell plasmon modes are shown schematically in this figure.

The thickness of the dielectric spacer layer, $|R_3 - R_2|$, controls the strength of the coupling between the inner and outer nano-shell. There is a strong coupling case when there is a small (28 nm) interlayer spacing between inner- and outer-metal shell layers, which leads to the close resonance of the inner and outer nano-shell plasmons, but this coupling weakens when the spacing between inner and outer metal layers is slightly increased (39 nm). Finally, there is a fully decoupled plasmon response when the inter-shell spacing is 236 nm [45, 49].

In a nano-shell, the local field inside the shell is significantly enhanced due to SPRs of both the inner and outer surfaces. Therefore, in a nano-matryushkas a considerable field enhancement can be obtained as the result of the collective coupling of surface plasmons
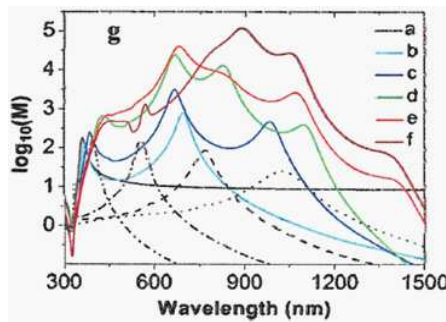
Figure 12. Enhancement factor at a distance of 0.25 nm away from the surface of the Ag core along the direction of the incident polarization versus the incident wavelength [50].

of the metal core and the metal shells, because the multilayered metal shells multiplicatively act as a group of effective optical condensers to focus the incident light toward the geometric centre. Then the focused light will excite the surface plasmon of the metal core and induce an extremely large local-field enhancement in the cavity between the metal core and the innermost metal shell [50]. Figure 12 shows how the enhancement factor 176 of a bare nano-sphere (Figure 12(a)) at = 398 nm can be increased to 776 at 690 nm, 31000 at 664 nm, and 400000 at 678 nm by adding 1, 2, and 4 extra metal shells to the nano-sphere (Figures 12(b)–(f)). The experiments also reveal that increasing the inner-shell distances, red-shifts the plasmon resonance [50].

3.2.7. Nano-particles on a Film

The interaction between localized plasmon of a nano-sphere with radius R and delocalized plasmon of a film with thickness T is controlled by adjusting the particle-film separation Z ($> R$) and film thickness T. This structure is shown in Figure 13.

Thus, three different interaction regimes are considered, (i) in the thick film case, $T > 2Z$, hybridization between the localized sphere plasmons and the sharp distribution of surface plasmons around ω_{SP} results in strong, localized, low- and high-energy plasmon states, (ii) in the intermediate film thicknesses, ($T \approx Z$), the nanosphere plasmon energies lie within the effective surface plasmon continuum, and (iii) in the thin film regime, ($T < Z/2$), the effective film continuum lies at lower energies than the discrete plasmons of the nano-sphere [45, 51].

In addition to the above real localized state of enhancement,
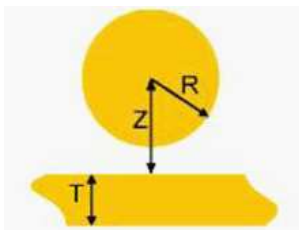
Figure 13. Schematic of the configuaration of nano-particle on a film [51].
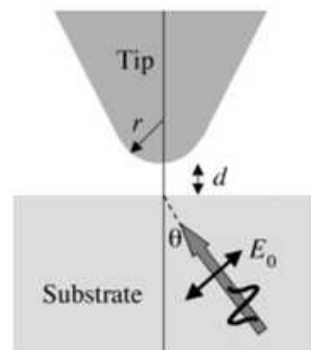
Figure 14. Section of a tip-surface substrate [36].

it has been shown that a virtual plasmon resonance composed of delocalized thin film plasmons can also be induced. Unlike the localized state, which is primarily composed of the discrete state, the virtual state is composed primarily of continuum states with only a small admixture of the discrete state. This state in a nano-particle on a film structure strongly depends on the incident light polarization, film thickness, and nanoparticle-film separation distance. Decreasing the thickness of the film tunes the virtual state to lower wavelengths. The large electromagnetic field enhancements induced across the junction between the nano-particle and the thin film in the case of the virtual state excitement, suggests applications for surface enhanced spectroscopies and surface enhanced scanning probe microscopies [52]. It has also been shown that the plasmonic behaviour of a metallic nano-shell near a metallic film depends on the aspect ratio of the nano-shell and the thickness of the film, which induces a low-energy virtual state [53].

3.3. LSPR Design Parameters, Sharp Tips Effect

Tip-surface is utilized in tip-enhanced Raman spectroscopy (TERS), for excitation of the LSPR as a scanning probe. This structure does not need any noble-metal substrates (Figure 14). Employing this structure using silver tip, enhancements of up to 10^{14} fold in the Raman signal have been claimed [54], which is the direct result of the above rule.

Experiments also show that the largest plasmon electric field for a perfect nano-trigonal occurs at the tips for the main plasmon resonance (dipole resonance), and at the sides for the second peak (quadrupole resonance). Furthermore, the quadrupole field pattern decays faster than that of the dipole polarization. Investigating the plasmon spectra of both perfect and snipped trigonal prisms (DDA modelling results) shows three peaks; the strongest one is in the visible range and very sensitive to triangular snipping. The more snipping, the more blue-shift in the main plasmon peak is observed; however, the two other peaks are pretty fixed with changing the snipping [29, 55].

3.4. LSPR Design Parameters, Aspect Ratio Effect

Increasing the aspect ratio of the nanoparticle when the incident light is polarized along the major axis of the nanoparticle, enhances the surface plasmon electric field, while shifting the dipole resonance wavelength towards red wavelength.

The PH method calculations also verify the above rules of the wavelength shift for the dipole resonance mode ($l = 1$) and higher multipolar modes ($l \geq 2$) in both longitudinal ($m = 0$) and transverse

($m = 1$) modes [56]. Based on the Voshchinnikov and Farafonov (VF) code [57], it has been shown that in longitudinal polarization as the aspect-ratio of a nano-rod increases, the dipole plasmon resonance gradually is red-shifted and the quadrupole resonance peak, which is larger than the dipole peak in a nano-sphere, is further faded [29]. It is also shown in Ref. [23] that the quadruple resonance presents an almost fixed oscillation of around 520 nm, which is the same as spherical nano-particles, but the dipole resonance strongly depends on the aspect ratio of the nano-rod. In addition, other investigations demonstrate that reducing the aspect ratio of a nano-ring red-shifts the plasmon resonance, and also reduces the extinction amplitude [58–60].

The interaction of a gold nano-rod in air on an ITO using the eigenmode approves that, as the aspect ratio of the nano-rod increases, the interaction decreases. Furthermore, the surface charges tend to remain clustered at the ends of the ellipsoid so that the fraction of the total area that interacts with the substrate decreases. As a result, effective background permittivity rises, and the depolarization factor decreases, resulting in a larger polarizability. This is expected, since the longer the nano-rod, the more needle-like it becomes, increasing its polarizability and dipole resonance [61].

FDTD modelling of an elongated rhombus in Figure 15(a) for fixed minor axis diameter of $b = 100$ nm, particle thickness of $h = 50$ nm, and various major axis diameter of $a = 100$–200 nm, demonstrates that dipolar plasmons are enhanced by increasing the aspect ratio when the particle elongation is along the polarization direction. However, Figure 15(b) shows that quadrupole extinction cross sections become more important by increasing the aspect ratio when the particle
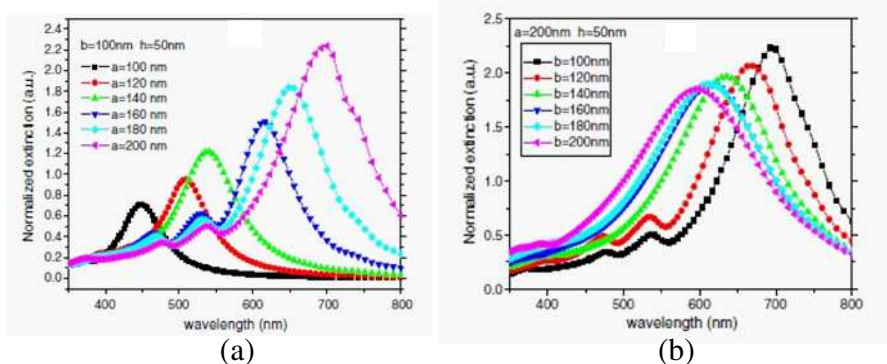

Figure 15. The effect of aspect ratio on dipolar and quadrupolar extinction cross section for elongated nano-rhombuses (a) along the polarization direction, (b) normal to the polarization direction [30].

elongation is normal to the polarization direction. This is valid for particles with similar major axis diameter and particle thickness but larger minor axis of $b = 200\,\text{nm}$ [30].

## 3.5. LSPR Design Parameters, Asymmetry Effect

Presenting asymmetry prevents using Mie theory. Figure 16 shows four topologically different Ag nano-rod structures. plasmon energy is calculated for these structures using the DDA method for p- and s-polarizations of electric fields.

(a) Needle (b) Peirodic cylinder (c) L-shape (d) Y-shape
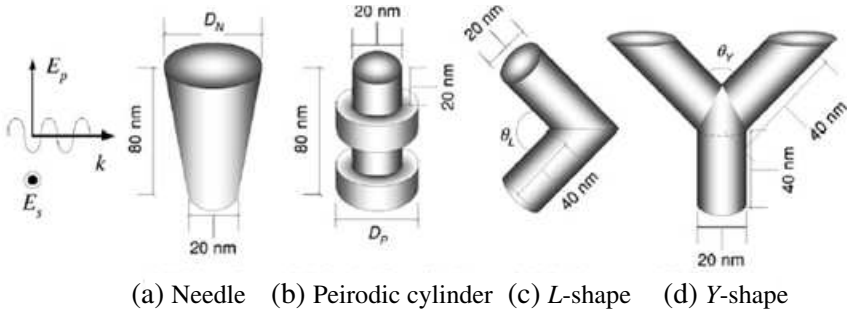
Figure 16. The schematics for four nano-rods topology [62].

It has been shown that in p-polarization, there is generally no strong peak relevant to quadrupole plasmons; however, these plasmons are highlighted mostly in s-polarization. In addition, increasing the asymmetry of the nano-particle, i.e., aspect ratio in the needle type, increasing the periodic asymmetries in the periodic one, decreasing the L-shaped corner angle θ_L, or increasing the Y-shaped angle θ_Y, dismisses the quadrupole plasmon from the extinction spectrum [62].

Figures 17(a) and (b) show two nano-shells with one and two pinholes, respectively. The effect of the defects on the E-fields, polarized along the y-axis (Figures 17(c) and (d)) presents a maximum enhancement factor of 320 at the pinhole locations, which is about 34 times that of the seamless nano-shells. However, for the polarization along the x-axis, the E-field enhancement at the pinholes is almost the same as that for the pinhole-free nano-shells [63]. If the number of bumps is increased, the magnitude of the extinction cross section increases, and the extinction cross section is broadened with a slightly larger red-shift and more pronounced broadening, due to the thinning of the nano-shell, which leads to a plasmon resonance red-shift [47]. The far-field extinction spectrum is remarkably insensitive to defects, but near-field properties are strongly influenced by localized defects.
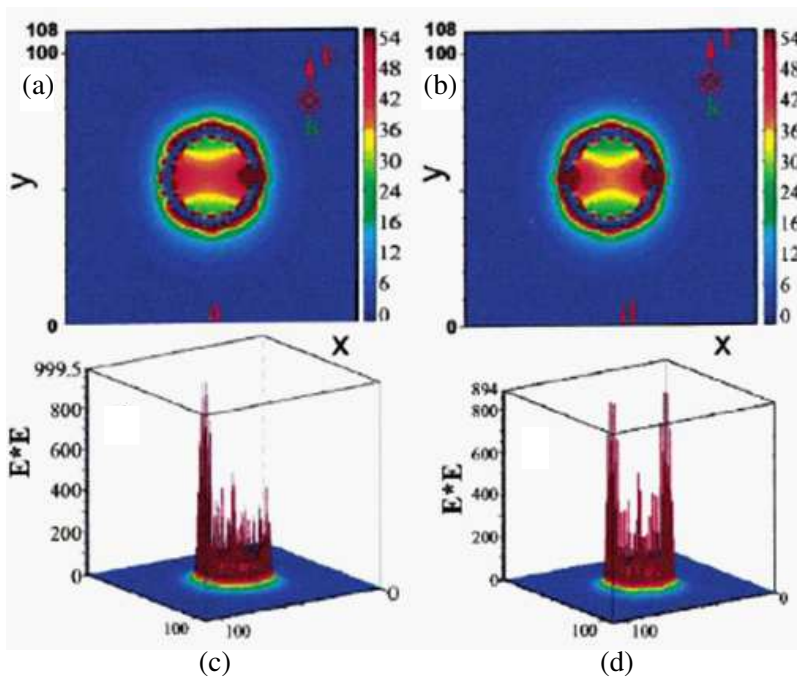
Figure 17. *E*-field enhancement for a Au nano-shell (18 nm in radii and 3 nm in thickness) with (a) one or (b) two pin-holes; 3-D plots of the enhanced field of (c) and (d) [63].

3.6. LSPR Design Parameters, Material Effect

The most common metals used in LSPR applications are silver (Al), gold (Au), copper (Cu), and aluminium. Silver and gold are more common than the others because of their high enhancement capability. Unlike silver, gold, and copper which have high threshold energy for interband activity, aluminium has a lower threshold of activity. Thus, aluminium can be used in the Drude model with high accuracy. In addition, copper and aluminium are abundant and cheap [24].

The real and imaginary parts of the electric permittivity for these four metals is shown in Figures 18(a), (b). Obviously, Cu and Au have almost similar permittivity values and the same interband thresholds of 2 eV, where their imaginary part of permittivity raises. Ag has a different threshold value for interband energy activation at 4 eV, and Al interband threshold happens at around 1.5 eV with much lower value for the real part of its permittivity. The LSPR resonance frequency depends on the real part of the permittivity, and resonance line width
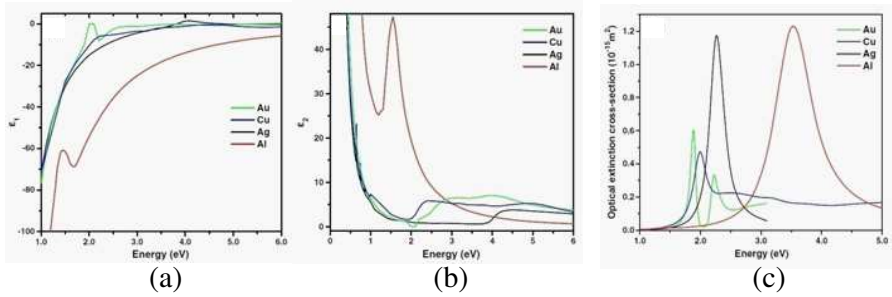
Figure 18. Effect of metal material on (a) real part of the electric permittivity, (b) imaginary part of the electric permittivity, and (c) plasmon extinction cross section [24].
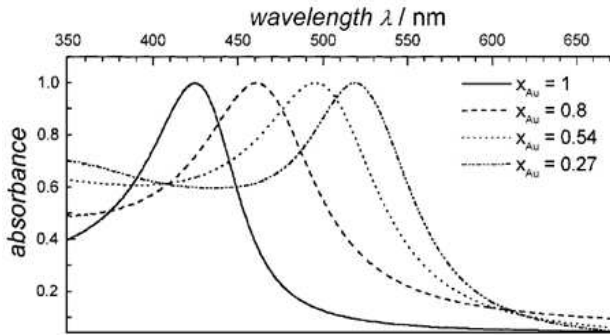
Figure 19. Variation of the surface plasmon absorption with alloy decomposition [23].

or spectrum flatness on its imaginary part. Thus, the smaller the real part of the permittivity is, the higher the plasmon frequency becomes (e.g., for Al); and the higher the interband threshold is, the sharper the spectrum becomes (e.g., for Ag). This rule has been explained in Figure 18(c).

Since reducing the Au content decreases the enhancement significantly [64], to keep the enhancement factor in the reasonable range, we need to have a higher plasmon wavelength. Figure 19 explains how reducing the silver content, red-shifts the plasmon frequency.

Increasing the environment dielectric factor red-shifts the plasmon resonance, causes stronger Fano resonance, and therefore more enhancements. This rule has been demonstrated for a silver-truncated tetrahedral nano-particle, based on both DDA numerical calculation method and experimental results [29].

The permittivity of the surrounding medium or refractive index per molecular binding, which is the second power of the permittivity, can be raised in at least three ways. First, larger molecules (e.g., proteins) produce larger shifts roughly in proportion to the mass of the molecule. Second, chromophores that absorb visible light couple strongly with the LSPR of nano-particles to produce large shifts and can be used to detect small molecules binding to protein receptors. Third, pairs of nano-particles that are separated by less than about 2.5 particle radii show plasmonic coupling and marked spectral shifts [4, 8].

In another research, the DDA calculations implemented by Schatz et al. to model a 10 nm silver sphere either sinking into a mica substrate or surrounded by free vacuum, demonstrates that the plasmon wavelength of the sphere gets red-shifted when the sphere goes from free vacuum to being partially embedded in the mica [29].

3.7. LSPR Design Parameters, Polarization Effect

Figures 20(a), (b) compare extinction efficiency of two single nano-spheres with radii of 30 and 60 nm, respectively, for two group points on the sphere, (a) along the polarization direction (point 1) and (b) rotated 45 degrees away from the polarization direction (point 2). It is obvious that the field enhancement for point 1 is much larger than that of point 2. It has been shown that the dimer enhancement is approximately four times as large as a single Ag sphere, for a parallel polarization of the incident wave. In contrast, perpendicular excitation of the dimer results in an enhancement factor below unity [65].

Also using the PH method, the nano-stars have been modelled as the hybridization of a solid core and the individual tips of the



(a) *R*=30 mm   (b) *R*=60 mm
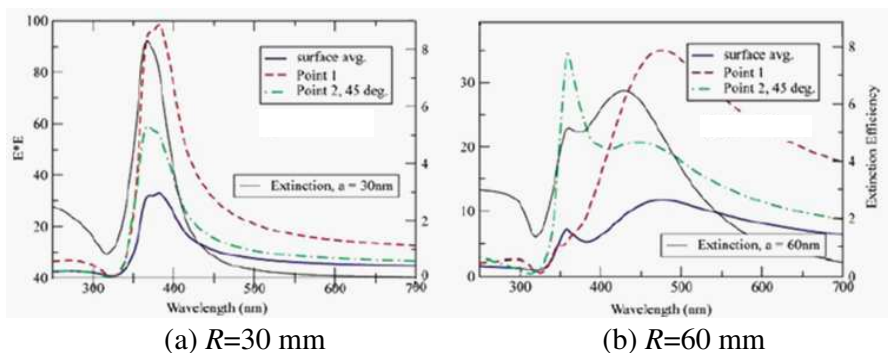
Figure 20. Comparison of extinction efficiency, for specific points for radius Ag spheres with radii of (a) 30 nm and (b) 60 nm [29].

particle. Figure 21(a) shows calculation results for an electric field with a polarization angle $\theta = 0°$, and wavelength of 804 nm, which shows a big plasmon resonance on the horizontal tip (1.9 eV), while the enhancement on other tips is very small. The results for a polarization angle $\theta = 60°$ (Figure 21(b)) exhibit a larger second resonance than the first one at 2.1 eV localized on the downward pointing tip. Finally, Figure 21(c) shows the enhancement results for a polarization angle $\theta = 90°$, where another resonances at 2.5 eV is seen at the two upward pointing tips.

Also it has shown that maximum value of Raman intensity for a dimer configuration is achieved for an incident polarized parallel to the dimer axis. The SERS intensity is well defined with respect to the polarization angles as $\cos^4(\alpha)$, where α is the incident angle with respect to the dimer axis. Although this equation is not sensitive to the particle size, incident wavelength, or interparticle separation, whenever the target molecules are immobilized on the particles; the absolute enhancement factor magnitude considerably depends on these factors [35].

The DDA modelling results of the metal right-handed helical Ag nanostructure, shown in Figure 22(a), for p-, s-, left-handed circular, and right-handed circular polarizations for two different circular radii $R = 20$ (Figure 22(b)) and 30 nm (Figure 22(c)).

As shown in Figures 20(b), (c), p-polarized electromagnetic wave introduces only one strong peak in the extinction spectrum, which is along the main axis. However, other polarizations produce two peaks in the spectrum; one of them is in the UV range due to the electron oscillation perpendicular to the cross section (quadrupole resonance), while the main absorbance peak in the visible range is due to the electron oscillation in the rod section tangent to the helix (dipolar resonance), which red-shifts with increasing helix radius. For larger
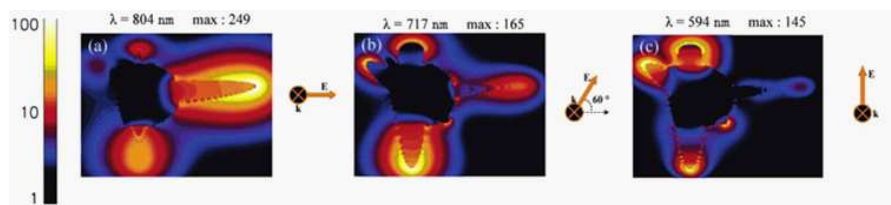
Figure 21. Maximum electric field enhancements for excitation of a nano-star with (a) 0-degree polarization, (b) 60-degree polarization, and (c) 90-degree polarization. The maximum field enhancements are indicated on top of each panel [55].
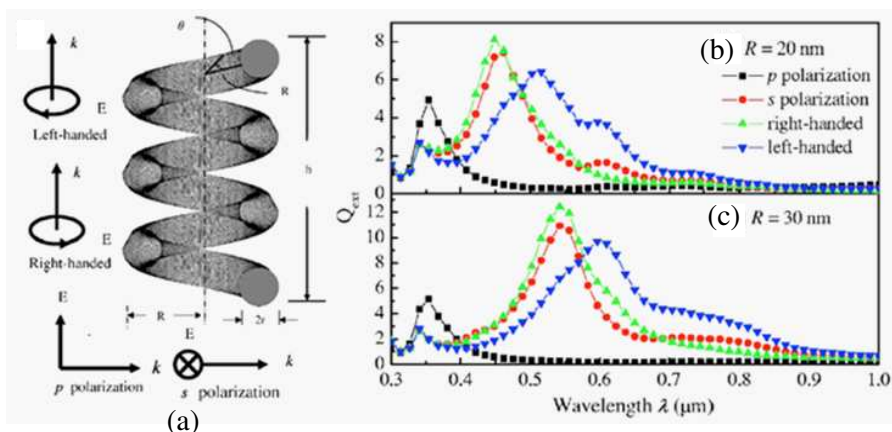
Figure 22. (a) Schematics for the right-handed helical Ag nanostructure. Calculated extinction spectra of Ag helical nanostructures for helix radii (b) $R = 20\,\text{nm}$ and (c) $R = 30\,\text{nm}$ [66].

radius of the helix, the maximum extinction is less than the smaller one, because of a weaker coupling inside the helix near the centre axis. For s-polarized light, the maximum E field is distributed around the center axis of the helix due to strong coupling; while with circular polarized light, the maximum E field is on the top or bottom, depending on the incident direction of the helix.

Investigating the optical properties of a metallic torus (nano-ring) for different shapes and different polarizations using the PH method also shows that for incident light polarized in the plane of the torus (i.e., along the main axis), the optical spectrum has a long wavelength highly tunable dipolar plasmon resonance, and a short wavelength mode corresponding to excitation of several higher order torus modes. While for perpendicular polarization, the spectrum exhibits a single feature made up of several closely spaced higher order torus modes which are only weakly dependent on the aspect ratio [67]. Also, the polarization effect on a nano-rod array (fabricated by OAD) shows that the plasmon energy spectrum of a nano-rod red-shifts and broadens in visible range when strikes with p-polarized light, but it has a sharp peak in the UV wavelength range [62].

4. DISCUSSION

As described in Section 3, nano-particles morphology and incident electromagnetic characteristics are very important for tuning plasmon

resonances. The effect of these parameters on plasmon resonance including the enhancement rate and wavelength shift of the excited multipolar plasmons, and the direction with maximum enhancement are summarized in Table 1.

Table 1. Parameters affecting the LSPR efficiency.

Parameters \ Effects	Dipole plasmon	Quadrupole plasmon	Comments
Intrinsic region size increase	Blue-shift, More enhancement		
Single particle, extrinsic region size increase	Red-shift, More enhancement	Blue-shift	
Nanostructures	More enhancement	Less enhancement	hemisphericals and cubiods have more enhamcement than dimers
Tip Sharpness increase (p-polarization)	Red-shift, More enhancement		Creation of dipole resonances on the tips, and quadrumors on the sides
Aspect ratio increase	Red-shift, More enhancement	Blue-shift, Less enhancement	polarization direction along the major axis
Aspect ratio decrease	Blue-shift, Less enhancement	Red-shift, More enhancement	polarization direction along the minor axis
Asymmetry (defects) increase	Red-shift, More enhancement	Blue-shift, Less enhancement	Mie theory not-usable
Particle-Substrate interaction increase	Red-shift, More enhancement	Blue-shift, More enhancement	using nano-pillars
Analyte or Environment permittivity increase	Red-shift	Red-shift	

Particle-Particle separation decrease (more interaction)	Red-shift, enhancement (plateaus after 3 times the particle size)		e.g., Separation in nano-structures, shell thickness and core diameter innano-shells, particle on metal film distance
Shells separation in nano-matryushkas decrease	More enhancement in lower wavelengths,		More dependence on inner shell spectrum for lower separation

As can be seen from the table, p-polarization creates more enhancement than other polarizations (when electric field vector direction is aligned with the major axis of the nano-particle). Moreover, increasing the aspect ratio more red-shifts the plasmon resonance for p-polarization, while fading the scattered wave at the same time. Conversely, increasing the aspect ratio for s-polarization waves more blue-shifts the resonance, while enhancing the extinction spectrum. Although the plasmon spectrum of single particles are scale invariant, but in multiparticle structures, increasing the particle size, and shrinking the particles gaps increase the enhancement of the extinction spectrum, and red-shift the resonance frequency. To increase hot spots due to particle-particle interactions, structures such as nano-shells and nano-matryushkas can be employed with the high tuneability capability. Unlike particle-particle interaction, decreasing particle-substrate interaction presents more enhancements in the extinction spectrum. To dismiss quadrupole and higher multipole effects, using p-polarized waves and larger nano-structured particles with further asymmetry is recommended. These asymmetries can be achieved with increasing aspect-ratio, or even with creating defects in the nano-particles structure, where hot-spots are considered in the defected areas. In addition, dimers have more dipole resonance components than trimers and quadrumors; in addition, dimer arrays present more enhancements than singular dimers. Sharp edges are best spots for surface charge accumulations and plasmon enhancement; thus, they can be utilized in the design of dimer hot-spot areas.

According to these observations, the following rules can be formulated which will help us in design of LSPR devices for the purpose of SERE biosensing,

- **Rule 1**, Unlike the intrinsic effect, the extrinsic effect increases the dipole plasmon wavelength with rising size r, while more

multipoles are presented in the extinction spectrum.

- **Rule 2**, The dipole enhancement has the highest value along the polarization angle ($\theta = 0$), Eq. (5), especially in smaller particles. However, increasing the size of the particle yields a more uniform extinction over the particle surface in different angles θ, while quadrupole enhancement is maximized in the direction normal to polarization angle.

- **Rule 3**, When light exposes a nano-particle, all odd multipole plasmon resonances are excited. The even ones are dark modes.

- **Rule 4**, Increasing the environment dielectric factor red-shifts the plasmon resonance, causes stronger Fano resonance, and therefore more enhancements.

- **Rule 5**, The coupling effect between nano-particles decrease for higher angular momentum orders as $D^{-(l+l'+1)}$.

- **Rule 6**, Dependence of nano-structured plasmons to the particle separations in the longitudinal mode (i.e., $m = 0$) is much more than the transverse mode ($m = 1$), because of the anisotropy of the multipolar interaction potential.

- **Rule 7**, Increasing the hot spot area considerably reduces the maximum enhancement, but this reduction plateaus for separations greater than three times the nano-sphere radius. Also, this increase causes the resonance frequency blue shifts.

- **Rule 8**, Nano-shells broaden and red-shift the spectrum of an isolated nano-particle. The smaller shell thickness or larger core diameter produces larger red-shift in the plasmon resonance.

- **Rule 9**, The plasmon energies of a nano-particle on a nano-film exhibit strong enhancements as the particle approaches the surface.

- **Rule 10**, Decreasing the spacing between the two shells in nano-matryushkas, mostly affects the low wavelength profile of the total plasmon resonance. However, when the separation increases, the total nano-shell plasmon spectrum more accurately follows the outer-shell plasmon spectrum.

- **Rule 11**, The surface charges desire to accumulate at the tip points; thus, the maximum enhancement occurs at sharp points, but quadrupole resonances are concentrated on plain sides. Therefore, the main plasmon energy peak of a tip enhances and red-shifts with increasing tip length or the sharpness of the tip. However, the enhancement drops dramatically as the distance between the tip and the substrate increases. The spatial resolution of TERS is also mainly dependent on the radius of curvature of the tip end [68].

- **Rule 12**, In longitudinal polarization case of the incident electric field, the more prolate is the nano-particle (along the polarization direction), the more red-shift occurs at dipolar plasmon frequencies (see Eqs. (11) and (12)), while in transverse polarization case of the incident electric field, the more prolate is the nano-particle (normal to the polarization direction), the more blue-shift occurs at the dipolar plasmon frequencies and the dipolar enhancement drops; however, other multipolar plasmon resonances grows with increasing aspect ratio (Eqs. (11) and (12)).
- **Rule 13**, Quadrupole resonances are quenched by increasing the particle asymmetry for p-polarization, but enhanced for s-polarization.
- **Rule 14**, Defects, which are another type of asymmetry, enhance and red-shift the electric field like hot spots, when the polarization of the incident light is parallel to the defect or asymmetry axis. However, they fade and blue-shift the electric field, when the polarization of the incident light is perpendicular to the defect or asymmetry axis.
- **Rule 15**, As the offset of nano-eggs increases, the optical spectrum broadens and includes additional red-shifted peaks and increasing asymmetry of the spectra.

5. CONCLUSION

In this article, we formulated a number of rules that explain the effects of morphological and electromagnetic parameters on the LSPR extinction spectrum based on various experimental and analytical published works. Researches can employ these rules to manipulate the morphological and electromagnetic parameters for optimally designing LSPR devices. Through this approach, the required sensitivity and accuracy can be granted prior to multiphysics modelling and then fabrication of the device.

REFERENCES

1. Mortazavi, D., A. Z. Kouzani, and A. Kaynak, "Nano-plasmonic biosensors — A review," *International Conference on Complex Medical Engineering*, Harbin, 2011.
2. Fleischmanna, M., P. J. Hendraa, and A. J. McQuillan, "Raman spectra of pyridine adsorbed at a silver electrod," *Chemical Physics Letters*, Vol. 26, No. 2, 163–166, 1974.

3. Stuart, D. A., C. R. Yonzon, X. Zhang, O. Lyandres, N. C. Shah, M. R. Glucksberg, J. T. Walsh, and R. P. van Duyne, "Glucose sensing using near-infrared surface-enhanced Raman spectroscopy Gold surfaces, 10-day stability, and improved accuracy," *Analytical Chemistry*, Vol. 77, 4013–4019, 2005.

4. Willets, K. A. and R. P. van Duyne, "Localized surface plasmon resonance spectroscopy and sensing," *The Annual Review of Physical Chemistry*, Vol. 58, 267–297, 2007.

5. Riboh, J. C., A. J. Haes, A. D. McFarland, C. R. Yonzon, and R. P. van Duyne, "A nanoscale optical biosensor real-time immunoassay in physiological buffer enabled by improved nanoparticle adhesion," *J. Physical Chemistry B*, Vol. 107, 1772–1780, 2003.

6. Mayergoyz, I. D., D. R. Fredkin, and Z. Zhang, "Electrostatic (plasmon) resonances in nanoparticles," *Physical Review B*, Vol. 72, 155412–155426, 2005.

7. Mishchenko, M. I., L. D. Travis, and J. W. Hovenier, *Light Scattering by Nonspherical Particles: Theory, Measurements, and Applications*, Academic Press, 2000.

8. Anker, J. N., W. P. Hall, O. Lyandres, N. Shah, J. Zhao, and R. P. van Duyne, "Biosensing with plasmonic nanosensors," *Nature Materials*, Vol. 7, 442–453, 2008.

9. Davis, T. J., K. C. Vernon, and D. E. Gómez, "Designing plasmonic systems using optical coupling between nanoparticles," *Physical Review B*, Vol. 79, 155423–155432, 2009.

10. Haynes, C. L., A. D. McFarland, and R. P. van Duyne, "Surface-enhanced Raman spectroscopy," *Analytical Chemistry*, 339–346, Sep. 1, 2005.

11. Politano, A., R. G. Agostino, E. Colavita, V. Formoso, and G. Chiarello, "Electronic properties of self-assembled quantum dots of sodium on Cu(111) and their interaction with water," *Surface Science*, Vol. 601, 2656–2659, 2007.

12. Politano, A., R. G. Agostino, E. Colavita, V. Formoso, and G. Chiarello, "High resolution electron energy loss measurements of Na/Cu(111) and H2O/Na/Cu(111) Dependence of water reactivity as a function of Na coverage," *J. of Chemical Physics*, Vol. 126, 244712, 2007.

13. Slaughter, L., W.-S. Chang, and S. Link, "Characterizing plasmons in nanoparticles and their assemblies with single particle spectroscopy," *J. of Physical Chemistry Letters*, Vol. 2, 2015–2023, 2011.

14. Angulo, A. M., C. Noguez, and G. C. Schatz, "Electromagnetic field enhancement for wedge-shaped metal nanostructures," *J. of Physical Chemistry Letters*, Vol. 2, 1978–1983, 2011.

15. Schatz, G. C. and R. P. van Duyne, *Electromagnetic Mechanism of Surface-enhanced Spectroscopy*, John Wiley & Sons Ltd., Chichester, 2002.

16. Whitney, A. V., J. W. Elam, S. Zou, A. V. Zinovev, P. C. Stair, G. C. Schatz, and R. P. van Duyne, "Localized surface plasmon resonance nanosensor a high-resolution distance-dependence study using atomic layer deposition," *J. Physical Chemistry B*, Vol. 109, No. 43, 20522–20528, 2005.

17. Kennedy, B. J., S. Spaeth, M. Dickey, and K. T. Carron, "Determination of the distance dependence and experimental effects for modified SERS substrates based on self-assembled monolayers formed using alkanethiols," *J. Physical Chemistry B*, Vol. 103, 3640–3646, 1999.

18. Stiles, P. L., J. A. Dieringer, N. C. Shah, and R. P. van Duyne, "Surface-enhanced Raman spectroscopy," *The Annual Review of Analytical Chemistry*, Vol. 1, 601–626, 2008.

19. Wang, D. S. and M. Kerker, "Enhanced Raman scattering by molecules adsorbed at the surface of colloidal spheroids," *Physical Review B*, Vol. 24, 1777–1790, 1981.

20. Kerker, M., D. S. Wang, and H. Chew, "Surface enhanced Raman scattering (SERS) by molecules adsorbed at spherical particles," *Applied Optics*, Vol. 19, No. 19, 3373–3388, 1980.

21. Payne, E. K., K. L. Shuford, S. Park, G. C. Schatz, and C. A. Mirkin, "Multipole plasmon resonances in gold nanorods," *J. Physical Chemistry B*, Vol. 110, 2150–2154, 2006.

22. Zhang, S., K. Bao, N. J. Halas, H. Xu, and P. Nordlander, "Substrate-induced Fano resonances of a plasmonic nanocube: A route to increased-sensitivity localized surface plasmon resonance sensors revealed," *Nano Letters*, Vol. 11, 1657–1663, 2011.

23. Link, S. and M. A. El-Sayed, "Spectral properties and relaxation dynamics of surface plasmon electronic oscillations in gold and silver nanodots and nanorods," *J. Physical Chemistry B*, Vol. 103, 8410–8426, 1999.

24. Sekhon, J. S. and S. S. Verma, "Rational selection of nanorod plasmons Material, size, and shape dependence mechanism for optical sensors," *Plasmonics*, Jan. 7, 2012.

25. Prangsma, J. C., *Local and Dynamic Properties of Light Interacting with Subwavelength Holes*, Amsterdam, Twente, 2009.

26. Yang, Z., Q. Li, F. Ruan, Z. Li, B. Ren, H. Xu, and Z. Tian, "FDTD for plasmonics: Applications in enhanced Raman spectroscopy," *Chinese Sceince Bulletin*, Vol. 55, No. 24, 2635–2642, 2010.

27. Dhawan, A., S. J. Norton, M. D. Gerhold, and T. Vo-Dinh, "Comparison of FDTD numerical computations and analytical multipole expansion method for plasmonics-active nanosphere dimers," *Optics Express*, Vol. 17, No. 12, 9688–9703, 2009.

28. Zeman, E. J. and G. C. Schatz, "An accurate electromagnetic theory study of surface enhancement factors for silver, gold, copper, lithium, sodium, aluminum, gallium, indium, zinc, and cadmium," *J. Physical Chemistry*, Vol. 91, No. 3, 634–643, 1987.

29. Kelly, K. L., E. Coronado, L. L. Zhao, and G. C. Schatz, "The optical properties of metal nanoparticles The influence of size, shape, and dielectric environment," *J. Physical Chemistry B*, Vol. 107, 668–677, 2003.

30. Zhou, X., M. Zhang, L. Yi, and Y. Fu, "Investigation of resonance modulation of a single rhombic plasmonic nanoparticle," *Plasmonics*, Vol. 6, 91–98, 2011.

31. Dmitriev, A., C. Hägglund, S. Chen, H. Fredriksson, T. Pakizeh, M. Käll, and D. S. Sutherland, "Enhanced nanoplasmonic optical sensors with reduced substrate effect," *Nano Letters*, Vol. 8, No. 11, 3893–3898, 2008.

32. Xu, H. and M. Käll, "Modeling the optical response of nanoparticle-based surface plasmon resonance sensors," *Sensors and Actuators B*, Vol. 87, 244–249, 2002.

33. Brandl, D. W., C. Oubre, and P. Nordlander, "Plasmon hybridization in nanoshell dimers," *J. of Chemical Physics*, Vol. 123, 024701–024711, 2005.

34. Prodan, E. and P. Nordlander, "Plasmon hybridization in spherical nanoparticles," *J. of Chemical Physics*, Vol. 120, No. 11, 5444–5454, 2004.

35. Xu, H. and M. Käll. "Polarization-dependent surface-enhanced Raman spectroscopy of isolated silver nanoaggregates," *ChemPhysChem*, Vol. 4, No. 9, 1001–1005, 2003.

36. Brown, R. J. C., J. Wang, and M. J. T. Milton, "Electromagnetic modelling of Raman enhancement from nanoscale structures as a means to predict the efficacy of SERS substrates," *J. of Nanomaterials*, Vol. 12086, 1–10, 2007.

37. Xu, H., J. Aizpurua, M. Käll, and P. Apell, "Electromagnetic contributions to single-molecule sensitivity in surface-enhanced

Raman scattering," *Physiacal Review E*, Vol. 62, No. 3, 4318–4324, 2000.

38. Gunnarsson, L., E. J. Bjerneld, H. Xu, S. Petronis, B. Kasemo, and M. Käll, "Interparticle coupling effects in nanofabricated substrates for surface-enhanced Raman scattering," *Applied Physics Letters*, Vol. 78, No. 6, 802–804, 2000.

39. De Garcia, A. F. J. and J. B. Pendry, "Collective theory for surface enhanced Raman scattering," *Physical Review Letters*, Vol. 77, No. 6, 1163–1166, 1996.

40. Brown, R. J. C., J. Wang, R. Tantra, Y. Re, and M. J. T. Milton, "Electromagnetic modelling of Raman enhancement from nanoscale substrates a route to estimation of the magnitude of the chemical enhancement mechanism in SERS," *Faraday Discussions*, Vol. 132, 201–213, 2006.

41. Schatz, G. C., M. A. Young, and R. P. van Duyne, *Electromagnetic Mechanism of SERS*, 19–45, Springer-Verlag, Berlin, Heidelberg, 2006.

42. Brandl, D. W., N. A. Mirin, and P. Nordlander, "Plasmon modes of nanosphere trimers and quadrumers," *J. Physical Chemistry B*, Vol. 110, 12302–12310, 2006.

43. Shegai, T., Z. Li, T. Dadosh, Z. Zhang, H. Xu, and G. Haran, "Managing light polarization via plasmon-molecule interactions within an asymmetric metal nanoparticle trimer," *PNAS*, Vol. 105, No. 43, 16448–16453, 2008.

44. Baer, R., D. Neuhauser, and S. Weiss, "Enhanced absorption induced by a metallic nanoshell," *Nano Letters*, Vol. 4, No. 1, 85–88, 2004.

45. Wang, H., D. W. Brandl, P. Nordlander, and N. J. Halas, "Plasmonic nanostructures artificial molecules," *Accounts of Chemical Research*, Vol. 40, No. 1 53–62, 2007.

46. Brandl, D. W. and P. Nordlander, "Plasmon modes of curvilinear metallic core-shell particles," *J. of Chemical Physics*, Vol. 126, 144708–144718, 2007.

47. Oubre, C. and P. Nordlander, "Optical properties of metallodielectric nanostructures calculated using the finite difference time domain method," *J. Physical Chemistry B*, Vol. 108, 17740–17747, 2004.

48. Radloff, C. and N. J. Halas, "Plasmonic properties of concentric nanoshells," *Nano Letters*, Vol. 4, No. 7, 1323–1327, 2004.

49. Prodan, E., C. Radloff, N. J. Halas, and P. Nordlander, "A hybridization model for the plasmon response of complex

nanostructures," *Science*, Vol. 302, No. 17, 419–424, 2003.

50. Xu, H., "Multilayered metal core-shell nanostructures for inducing a large and tunable local optical field," *Physical Review B*, Vol. 72, No. 073405, 1–4, 2005.

51. Le, F., N. Z. Lwin, J. M. Steele, M. Ka, N. J. Halas, and P. Nordlander, "Plasmons in the metallic nanoparticle-film system as a tunable impurity problem," *Nano Letters*, Vol. 10, No. 5, 2009–2013, 2005.

52. Nordlander, P. and P. Le, "Plasmonic structure and electromagnetic field enhancements in the metallic nanoparticle-film system," *Applied Physics B*, Vol. 84, 35–41, 2006.

53. Le, F., N. Z. Lwin, N. J. Halas, and P. Nordlander, "Plasmonic interactions between a metallic nanoshell and a thin metallic film," *Physical Review B*, Vol. 76, No. 165410, 1–12, 2007.

54. Richards, D., R. G. Milner, F. Huang, and F. Festy, "Tip-enhanced Raman microscopy practicalities and limitations," *J. of Raman Spectroscopy*, Vol. 34, 663–667, 2003.

55. Hao, F., C. L. Nehl, J. H. Hafner, and P. Nordlander, "Plasmon resonances of a gold nanostar," *Nano Letters*, Vol. 7, No. 3, 729–732, 2007.

56. Willingham, B., D. W. Brandl, and P. Nordlander, "Plasmon hybridization in nanorod dimers," *Applied Physics B*, Vol. 93, 209–216, 2008.

57. Voshchinnikov, N. V. and V. G. Farafonov, "Optical properties of spheroidal particles," *Astrophysics and Space Science*, Vol. 204, No. 1, 19–85, 1993.

58. Aizpurua, J., P. Hanarp, D. S. Sutherland, M. Kall, G. W. Bryant, and A. F. J. de Garcia, "Optical properties of gold nanorings," *Physical Review B*, Vol. 90, No. 5, 0574011–0574014, 2003.

59. Mayergoyz, I. D. and Z. Zhang, "Modeling of the electrostatic (plasmon) resonances in metallic and semiconductor nanoparticles," *J. of Computational Electronics*, Vol. 4, 139–143, 2005.

60. Mayergoyz, I. D. and Z. Zhang, "The computation of extinction cross sections of resonant metallic nanoparticles subject to optical radiation," *IEEE Trans. on Magnetics*, Vol. 43, No. 4, 1681–1684, 2007.

61. Vernon, K. C., A. M. Funston, C. Novo, D. E. Gomez, P. Mulvaney, and T. J. Davis, "Influence of particle-substrate interaction on localized plasmon resonances," *Nano Letters*, Vol. 10, 2080–2086, 2010.

62. Zhang, Z. Y. and Y. P. Zhaoa, "Tuning the optical absorption properties of Ag nanorods by their topologic shapes: A discrete dipole approximation calculation," *Applied Physics Letters*, Vol. 89, 023110–023112, 2006.

63. Hao, E., S. Li, R. C. Bailey, S. Zou, G. C. Schatz, and J. T. Hupp, "Optical properties of metal nanoshells," *J. Physical Chemistry B*, Vol. 108, 1224–1229, 2004.

64. Byun, K. M., D. Kimb, and S. J. Kima, "Investigation of the profile effect on the sensitivity enhancement of nanowire-mediated localized surface plasmon resonance biosensors," *Sensors and Actuators B*, Vol. 117, 401–407, 2006.

65. Xu, H., E. J. Bjerneld, M. Käll, and L. Börjesson, "Spectroscopy of single hemoglobin molecules by surface enhanced Raman scattering," *Physical Review Letters*, Vol. 21, No. 83, 4357–4360, 1999.

66. Zhang, Z. Y. and Y. P. Zhaoa, "Optical properties of helical Ag nanostructures calculated by discrete dipole approximation method," *Applied Physics Letters*, Vol. 90, 221501–221503, 2007.

67. Dutta, C. M., T. A. Ali, D. W. Brandl, T. H. Park, and P. Nordlander, "Plasmonic properties of a metallic torus," *J. of Chemical Physics*, Vol. 129, 084706–084714, 2008.

68. Yang, Z., J. Aizpurua, and H. Xu, "Electromagnetic field enhancement in TERS configurations," *Journal of Raman Spectroscopy*, Vol. 40, No. 10, 1343–1348, 2009.